IEEE Access
Multidisciplinary | Rapid Review | Open Access Journal

IEEE MAGNETICS SOCIETY SECTION

Received 17 August 2023, accepted 12 September 2023, date of publication 5 October 2023, date of current version 10 October 2023.

Digital Object Identifier 10.1109/ACCESS.2023.3317438

RESEARCH ARTICLE

Nonlinear Dynamic Characteristic Analysis Method Based on Load Angle of Two-Stage Magnetic Gearbox for Wind Turbine

QINGHAI QIN, BIN CAI, AND YUCHENG DU
College of Engineering, Qufu Normal University, Rizhao 276826, China

Corresponding author: Bin Cai (bincai1027@qfnu.edu.cn)

This work was supported in part by the National Natural Science Foundation of China under Grant 61473170, and in part by the Natural Science Foundation of Shandong Province under Grant ZR2023ME069 and Grant ZR2022MF224.

ABSTRACT The magnetic gearbox for wind turbine has the potential virtue of less maintenance, improved reliability, and overload protection. Dynamic performance analysis plays a key role in its optimal design and ensuring its stable operation. But so far, there are few unified and effective methods for dynamic performance analysis of magnetic gearbox especially for multistage magnetic gearbox. Thus, a nonlinear dynamic analysis method based on load angle is proposed for two-stage magnetic gearbox in this paper. First, the nonlinear dynamic model of two-stage magnetic gearbox is established based on load angle. Second, the analytical expressions of load angle and magnetic torque of magnetic gearbox facing instantaneous shock are obtained by Taylor expansion based on load angle. Third, the dynamic performance of magnetic gearbox under different operating conditions is analyzed. Finally, the simulation results are discussed, and the results show that the accuracy of the proposed analytical method is comparable to that of Runge-Kutta method, which verifies the effectiveness of the proposed method and facilitates its application to the fast dynamic evaluation and optimal design of multistage magnetic gearbox.

INDEX TERMS Dynamic characteristic, magnetic gearbox, load angle, Taylor expansion, Runge-Kutta method, wind turbine.

I. INTRODUCTION

In the transmission system of the doubly-fed and semi-direct drive wind turbines, the gearbox is one of the most critical components and its performance directly affects the stable operation of the wind turbines. The existing wind power gearbox (Fig.1) adopts mechanical gear transmission mode, it has the intrinsic disadvantages of high failure rate, high operation, and maintenance cost and so on, which seriously restricts the progression of high-power wind turbines [1], [2], [3]. Recently, due to the potential advantages of overload protection, high reliability, low maintenance cost, and low noise [4], [5], [6], the coaxial magnetic gear (CMG) [7] has received increasing attention in its application of wind power [8], [9], [10]. For instance, several attractive magnetic gearboxes for wind turbine (WMGB) and pseudo direct-drive machines (Fig.2) with different topological structures based on CMGs have been proposed for wind power generation [11], [12], [13].

Unlike conventional CMG which input load is relatively stable, although WMGB can achieve higher gear ratio, the input load of WMGB has the stochastic time-varying characteristic, as the wind speed and direction change randomly, especially the gust and turbulence, which seriously threatens the reliable operation of the transmission system [14]. Thus, it is necessary to ascertain the dynamic characteristic by enhancing the dynamic response research of the WMGB coupling transmission chain, so that the mechanical structure of WMGB can be further optimized to improve its dynamic operating performance. Furthermore, it is convenient to evaluate the feasibility of its application to high-power wind power generation system.

The associate editor coordinating the review of this manuscript and approving it for publication was Diana Leitao.

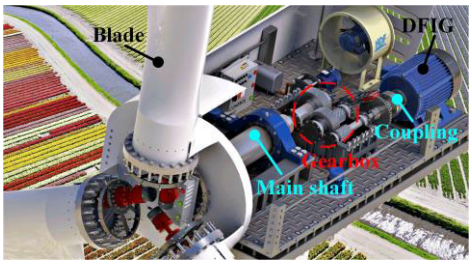

FIGURE 1. Conventional doubly fed wind turbine drive system.

FIGURE 2. Magnetically geared generator for wind turbines.

The lumped parameter method and finite element method (FEM) are usually used for the dynamic characteristics analysis of the mechanical gearboxes [15], [16]. They respectively consider the supports and the key components as flexible bodies to evaluate the local structural deformation under external forces. The above analysis methods provide useful references for the dynamic characteristics study of WMGB. However, different from mechanical gearboxes, the rotors of WMGB transmit torque through non-contact magnetic force. When facing time-varying loads, the problem of insufficient stiffness is inevitable [14]. Therefore, for WMGB, it is necessary to focus on the position angle and torque response of the rotors, rather than its local structural deformation.

The research on dynamic characteristics of CMG and its integrated machine are attracting more and more attention. A nonlinear dynamic evaluation method about CMG is performed by using the principle of superposition and energy conservation, but the solving accuracy will decrease with the increase of the torque ripple [8]. The potential transfer characteristic, nonlinear damping in motion control servo systems under overload conditions were investigated by theoretical analysis and experimental verification [17]. Chen and Tsai [18] developed a block diagram modeling method to predict the dynamic characteristics of CMG, which facilitates researchers to apply the method to a wider range of control applications directly. A fast and efficient procedure was proposed to simulate the dynamical response of CMG by obtaining the torque for every position angle and geometric configuration using Maxwell Stress Tensor [19]. The dynamic characteristics of CMG was investigated based on a 2-D analytical model and motion equations, and the effect of loading condition on the dynamic pull-out torque of CMG was also studied [20]. In [21], a dynamic model of the CMG control system is proposed to optimize the power transmission by combining the transient FEM and kinematic losses model. In [22], the transient performance of magnetically geared induction motor for a direct start was studied by numerical simulation. A dynamic analytical model of a particular magnetic gear based on pure dipole-dipole coupling was proposed by considering two types of friction in the bearing [23]. In addition, some researchers have also studied the dynamic characteristics of magnetic gears based on the lumped parameter method and FEM [24], [25].

However, the power transmitted by these magnetic gears is still relatively low, and there is little research on MW-scale WMGB system especially its dynamic characteristic analysis. In [14], the dynamic characteristic of the low-speed magnetic gear of a 1.5MW multistage WMGB under different wind speeds was analyzed. Desvaux et al. [26] proposed an analytical expression of magnetic torque under small step disturbance and defined various criteria to evaluate the dynamic performance. To simplify the analysis model, the concept of load angle is introduced into the motion equation [8], [16], [18]. The definition of load angle is the difference of the electrical or mechanical angle between the input and output rotors, which reduces the degree of freedom of system by variable substitution. Nevertheless, the existing research have almost focused on single CMG, or only for a specific operation condition. They have neither provided the dynamic information of WMGB with multistage CMGs under different operating conditions, nor a unified dynamic response expression.

Therefore, this paper focuses on the high-power WMGB with two-stage CMGs (Fig.3) and aims to provide a unified and effective nonlinear dynamic characteristic analysis approach. Furthermore, the dynamic performance of the proposed two-stage WMGB under different operating conditions will be analyzed to verify the effectiveness of the proposed method and the rationality of the two-stage WMGB applying to the wind power generation system.

The remainder of the paper is organized as follows: the nonlinear dynamic model of the two-stage WMGB transmission system is established in Section II. Then, the dynamic response expressions of load angle and magnetic torque based on the dynamic model of load angle Taylor expansion are given in Section III. Section IV analyzes a high-power WMGB to evaluate the effectiveness of the proposed analysis method and the influence of operating conditions on the dynamic performance of the system. Last, the conclusion is drawn in Section V.

II. DYNAMIC MODELING OF TWO –STAGE WMGB

A. OPERATING PRINCIPLE OF THE WMGB

As shown in Fig. 3, the two-stage WMGB transmission system contains two stages of CMG: the first-stage CMG (FSMG) and second-stage CMG (SSMG). The CMG (Fig.4) at different stages consists of the stator, inner rotor, and

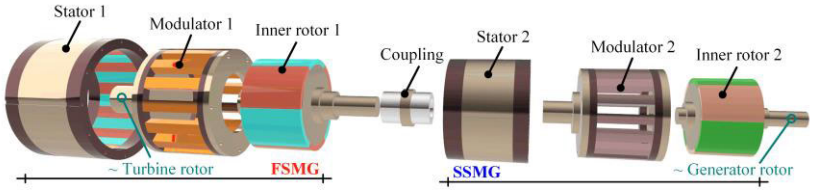

FIGURE 3. Two-stage WMGB transmission system.

modulator. The modulator of the FSMG is connected to the wind wheel via main shaft, and the inner rotor of the SSMG is connected to the generator via a coupling. The two-stage WMGB is designed for a 1.5 MW wind turbine, and its main system parameters are listed in Table 1.

For each CMG shown in Fig. 3, the pole-pair numbers of inner rotor and stator and the number of ferromagnetic segments must follow the relation (1) [10] and the gear ratio is given by Eq. (2).

$$N_{s\kappa} = p_{i\kappa} + p_{o\kappa} \tag{1}$$

$$G_\kappa = N_{s\kappa} / p_{i\kappa}, \quad G = G_1 G_2 \tag{2}$$

where, $\kappa = 1, 2$, represent FSMG and SSMG, respectively; $p_{i\kappa}$ and $p_{o\kappa}$ are the pole-pair numbers of the inner rotor and stator of the κ^{th} CMG, respectively; $N_{s\kappa}$ is the ferromagnetic segment numbers of modulator of the κ^{th} CMG; G_κ is the gear ratio of the κ^{th} CMG; G is the total gear ratio of WMGB.

Due to the existence of modulator, magnetic fields excited by the PMs on the inner rotor and stator respectively can be coupled effectively, such that abundant space harmonics are established in the inner and outer air-gaps. The radial flux density at a radial distance r established by PMs on inner rotor or stator can be expressed as follows:

$$\begin{aligned} &B_{r\phi}(r,\theta) \\ &= \Lambda_{r0} \sum_{m=1,3,5\cdots} b_{rm}(r) \cos\left(mp_\phi\left(\theta - \omega_\phi t\right) + mp_\phi\theta_0\right) \\ &\quad + \frac{1}{2} \sum_{m=1,3,5\cdots} \sum_{n=1,2,3\cdots} \Lambda_{rn}(r)\, b_{rm}(r) \cos \\ &\quad \times \left(\left(mp_\phi + nN_s\right) + \left(\theta - \frac{mp_\phi\omega_\phi + nN_s\omega_s}{mp_\phi + nN_s}\right) t + mp_\phi\theta_0\right) \\ &\quad + \frac{1}{2} \sum_{m=1,3,5\cdots} \sum_{n=1,2,3\cdots} \Lambda_{rn}(r)\, b_{rm}(r) \cos \\ &\quad \times \left(\left(mp_\phi - nN_s\right) + \left(\theta - \frac{mp_\phi\omega_\phi - nN_s\omega_s}{mp_\phi - nN_s}\right) t + mp_\phi\theta_0\right) \end{aligned} \tag{3}$$

and the circumferential flux density at r established by PMs on inner rotor or stator can be expressed as follows:

$$\begin{aligned} &B_{\theta\phi}(r,\theta) \\ &= \Lambda_{\theta 0} \sum_{m=1,3,5\cdots} b_{\theta m}(r) \sin\left(mp_\phi\left(\theta - \omega_\phi t\right) + mp_\phi\theta_0\right) \\ &\quad + \frac{1}{2} \sum_{m=1,3,5\cdots} \sum_{n=1,2,3\cdots} \Lambda_{\theta n}(r)\, b_{rm}(r) \sin \\ &\quad \times \left(\left(mp_\phi + nN_s\right) + \left(\theta - \frac{mp_\phi\omega_\phi + nN_s\omega_s}{mp_\phi + nN_s}\right) t + mp_\phi\theta_0\right) \\ &\quad + \frac{1}{2} \sum_{m=1,3,5\cdots} \sum_{n=1,2,3\cdots} \Lambda_{\theta n}(r)\, b_{\theta m}(r) \sin \\ &\quad \times \left(\left(mp_\phi - nN_s\right) + \left(\theta - \frac{mp_\phi\omega_\phi - nN_s\omega_s}{mp_\phi - nN_s}\right) t + mp_\phi\theta_0\right) \end{aligned} \tag{4}$$

where, ϕ can be i or o, they denote the inner rotor or stator, respectively; ω_ϕ is the rotational speed of the inner rotor or stator (of course, here $\omega_o = 0$), and ω_s is the rotational speed of modulator; b_{rm} and $b_{\theta m}$ are the radial and circumferential components of the flux density distribution without modulator; Λ_{r0}, Λ_{rn}, $\Lambda_{\theta 0}$ and $\Lambda_{\theta n}$ are the Fourier coefficients of modulating effect to the radial and circumferential components of the flux density, respectively. θ_0 is the initial mechanical angle.

The magnetic torque of the inner rotor and stator T_i and T_o can be obtained by calculated as follows:

$$T_i = \frac{L_{ef} r_i^2}{\mu_0} \int_0^{2\pi} B_{r\_i} B_{\theta\_i} d\theta \tag{5}$$

$$T_o = \frac{L_{ef} r_o^2}{\mu_0} \int_0^{2\pi} B_{r\_o} B_{\theta\_o} d\theta \tag{6}$$

TABLE 1. Parameters of two-stage WMGB transmission system.

Symbol	Parameter	Value
P_N	Nominal power	1.5MW
ω_N	Rated input speed	17.40r/min
T_{N1}/T_{N2}	Nominal torque of FSMG/SSMG	823.22/105.84kNm
T_{M1}/T_{M2}	Stall torque of FSMG/SSMG	987.86/127.01kNm
p_{i1}/p_{i2}	Pole-pair numbers of FSMG/SSMG's inner rotor	9/9
p_{o1}/p_{o2}	Pole-pair numbers of FSMG/SSMG's stator	61/76
N_{s1}/N_{s2}	Ferromagnetic segment Numbers of FSMG/SSMG's modulator	70/85
J_l	Inertia of LS motion rotor	3.8×10^4 kg.m^2
J_m	Inertia of MS motion rotor	4.0×10^4 kg.m^2
J_h	Inertia of HS motion rotor	5.0×10^3 kg.m^2

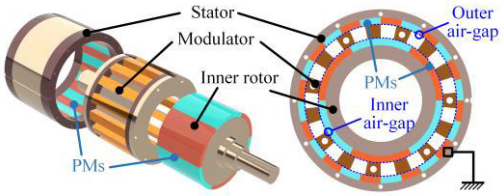

FIGURE 4. Single-stage CMG (FSMG) in exploded drawing.

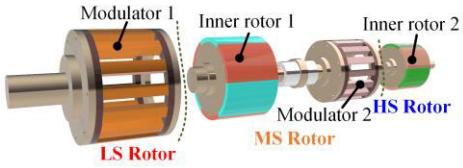

FIGURE 5. WMGB transmission system motion rotor division.

where, L_{ef} is the axial length of the CMG; μ_0 is the permeability of the vacuum; r_i and r_o are the circle radius of the inner and outer air-gaps, respectively; B_{r_i} and B_{θ_i} are the radial and tangential components of magnetic flux density in inner air-gap; B_{r_o} and B_{θ_o} are the radial and tangential components of magnetic flux density in outer air-gap, respectively.

According to the conservation of energy and mechanical balance, the magnetic torque of modulator is expressed as

$$T_s = -T_i - T_o \tag{7}$$

Under the unstable state, the magnetic torque of the modulator is related to the difference between the electrical angles of the modulator and inner rotor.

B. NONLINEAR DYNAMIC MODELING OF THE WMGB

According to the different rotation speeds of each component, the two-stage WMGB transmission system is divided into three rotors as shown in Fig. 5: low-speed (LS) rotor (i.e. FSMG's modulator), medium-speed (MS) rotor (i.e. FSMG's inner rotor and SSMG's modulator) and high-speed (HS) rotor (i.e. SSMG's inner rotor).

To facilitate the analysis, the following assumptions are made:

1) The mechanical structural design is relatively effective, and the friction of each rotor can be ignored;

2) The cogging torque is not considered, because it only affects the local dynamic behavior and its value is relatively small;

3) The shaft is completely rigid, and the torsional force at the shaft end is not considered;

4) The final purpose is to obtain the relationship between system response and system parameters, so the influence of the torque controller is not considered (or the torque is well controlled) here.

According to Newton's second law, the coupled motion equation of the transmission system can be expressed by

$$\begin{cases} J_l\ddot{\theta}_l + T_{M1}\sin\delta_1 = T_w \\ J_m\ddot{\theta}_m - G_1^{-1}T_{M1}\sin\delta_1 + T_{M2}\sin\delta_2 = 0 \\ J_h\ddot{\theta}_h - G_2^{-1}T_{M2}\sin\delta_2 = T_e \end{cases} \tag{8}$$

where, J_l, J_m and J_h are the inertia of LS, MS and HS rotors; θ_l, θ_m and θ_h are the mechanical angle of LS, MS and HS rotors; T_w and T_e are the driving torque of the wind turbine and the electromagnetic torque of the generator, respectively; T_{M1} and T_{M2} are the stall torque of FSMG and SSMG; $T_{M1}\sin\delta_1$ and $T_{M2}\sin\delta_2$ reflect the changes in the magnetic torque of FSMG and SSMG, respectively; δ_1 and δ_2 are the load angle of FSMG and SSMG respectively, i.e. the electrical angle difference between the modulator and inner rotor of CMG (taking δ_1 as an example, its annotation is shown in Fig. 6), which can be expressed as follows:

$$\delta_1 = N_{s1}\theta_l - p_{i1}\theta_m, \quad \delta_2 = N_{s2}\theta_m - p_{i2}\theta_h \tag{9}$$

When the system operates stably, the angular acceleration of each rotor is 0, so the stable operating points of FSMG and SSMG can be calculated according to Eq. (8):

$$\delta_{10} = \arcsin(T_w / T_{M1}) \tag{10}$$

$$\delta_{20} = -\arcsin(G_2T_e / T_{M2}) = \arcsin(G_1^{-1}T_{M1} / T_{M2}\sin\delta_{10}) \tag{11}$$

Generally, the modulator of FSMG suffers the random load from the turbine rotor, and its dynamic performance will directly affect the reliable operation of the transmission system. Further, to obtain the magnetic torque transmission characteristics of FSMG, as shown in Fig. 6, a 2D FEM was established in Ansys/Maxwell 2D and the detailed structure parameters are listed in [14]. Fig. 7 shows the curve of magnetic torque of input rotor changing with load angle δ_1 obtained by finite element analysis (FEA) and Eq. (8). And from Fig. 7, the results obtained by Eq. (8) are highly consistent with that of 2D FEA, which also shows the accuracy to describe the dynamic magnetic torque of FSMG by Eq. (8). Next, the torque ripple of the modulator and inner rotor of FSMG with different load angle calculated by 2D FEA are shown in Fig. 8. It can be seen from Fig.8 that the torque ripple of modulator is lower than that of inner rotor. If the load angle is around 0° (360°) or 180°, the torque ripple of the modulator and inner rotor reaches the maximum value. At this time, the FSMG in the light load state, thus the wind turbine in the shutdown state.

In addition, if the load angle is around 90° or 270°, the torque ripple of both modulator and inner rotor reaches the lower values (no more than 5%). However, once the load torque exceeds the stall torque of FSMG, the modulator will immediately decouple from inner rotor to realize overload protection. It means that the states corresponding to the above load angles are unstable in the engineering. Therefore, it is necessary to choose a suitable overload capacity to make CMGs operate in the stable area.

To further illustrate the evolutionary relationship of load angle, the curves of different types of angles with time under

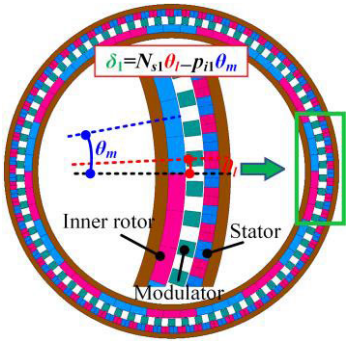

FIGURE 6. 2D FEM model of FSMG established in Ansys.

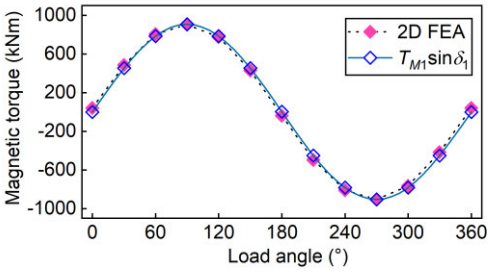

FIGURE 7. Curve of magnetic torque changing with load angle of FSMG.

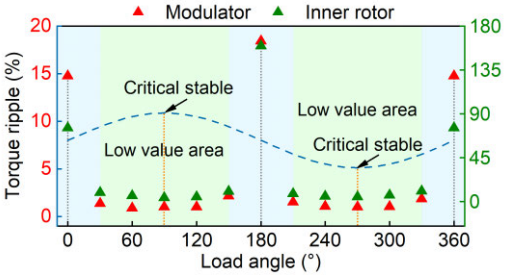

FIGURE 8. Torque ripple of modulator and inner rotor of FSMG.

rated operating conditions are shown in Fig. 9 to Fig. 11. Besides, the evolutionary relationship among different types of angles is elaborated in Fig. 12.

To observe the changes of all types of angles clearly, the sinusoidal angular velocity disturbance with amplitude of 0.02% and 0.1% is applied to the input and output rotors of WMGB, respectively. From Fig. 10(a) and 10(b), the electrical angles of modulator and inner rotor are a series of sawtooth shock pulses. However, due to short switching period and full angle range, it is difficult to determine the operating state of CMGs, which also makes difficulties for further quantitative analysis of the system dynamic performance.

Thus, the load angles are introduced to amplify evolutionary behavior of electrical angles by analyzing the difference of the electrical angles. Meanwhile, from Fig. 11, the load angle fluctuates in a tiny range near the constant stable operating point δ_{10} and δ_{20}, which is convenient for further

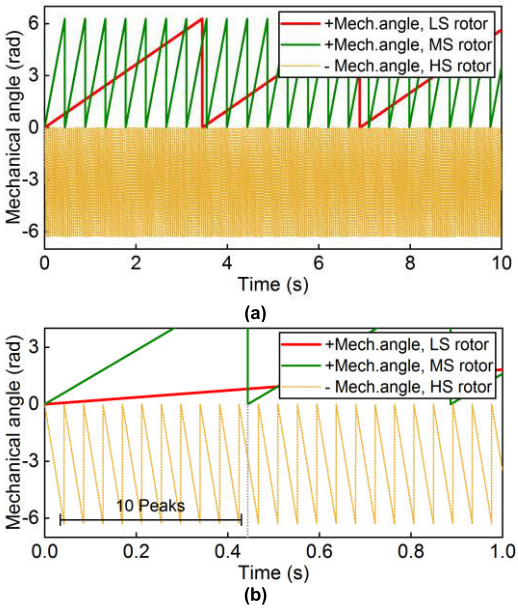

FIGURE 9. Mechanical angle waveforms of different rotors. (a) 0-10s, (b) 0-1s enlarged views.

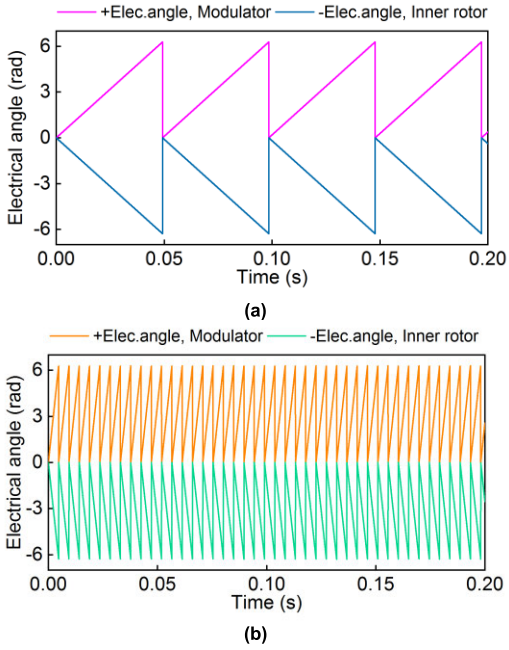

FIGURE 10. Electrical angle waveforms of different rotors. (a) FSMG, (b) SSMG.

evaluating the dynamic performance of the system via the range of the fluctuation.

Then, Eq. (8) can be transformed to:

$$\begin{cases} \ddot{\delta}_1 + T_{M11}\sin\delta_1 - T_{M22}\sin\delta_2 = T_{w\_eq} \\ \ddot{\delta}_2 - T_{M12}\sin\delta_1 + T_{M21}\sin\delta_2 = T_{e\_eq} \end{cases} \tag{12}$$

with,

$$T_{M11} = \left(N_{s1}/J_l + p_{i1}/(G_1 J_m)\right) T_{M1},$$
$$T_{M12} = \left(N_{s2}/(G_1 J_m)\right) T_{M1}$$

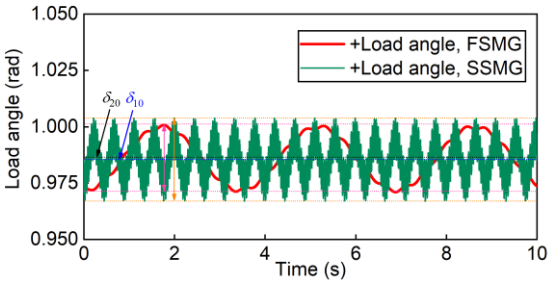

FIGURE 11. Load angle waveforms of different CMGs.

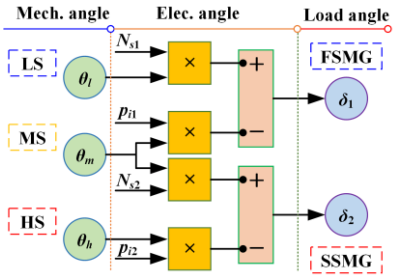

FIGURE 12. Evolutionary relationship among different angles in WMGB.

$$
\begin{aligned}
T_{M21} &= \left(N_{s2}/J_m + p_{i2}/(G_2 J_h)\right) T_{M2}, \\
T_{M22} &= \left(p_{i1}/J_m\right) T_{M2} \\
T_{w\_eq} &= N_{s1}/J_l \cdot T_w, \quad T_{e\_eq} = p_{i2}/J_h \cdot T_e
\end{aligned}
$$

In conclusion, the introduction of load angle has the following advantages for nonlinear dynamic characteristic analysis of the transmission system:

1) The degree of freedom of the original motion equation is reduced, and the analytical model is simplified from Eq. (8) to Eq. (12). Further, it is convenient for control research considering the entire wind power generation system in the future.

2) From Fig. 10, the original high frequency oscillation response is transformed into a low frequency constant response, which is convenient for analysis.

3) With strong scalability, relevant criteria can be defined to evaluate the dynamic performance of the system based on the above analysis. And the relevant details will be discussed in the following Sections.

III. ANALYTIC EXPRESSION OF DYNAMIC PERFORMANCE

A. MOTION EQUATION BASED ON TAYLOR EXPANSION OF LOAD ANGLE

To obtain the asymptotic solution of Eq. (12), the load angle δ_κ can be expanded into first-order Taylor series at the operating point $\delta_{\kappa 0}$:

$$
\sin\delta_\kappa = f_{\kappa 0} + f_{\kappa 1}\delta_\kappa + o(\delta_\kappa) \tag{13}
$$

with, $f_{\kappa 0} = \sin\delta_{\kappa 0} - \delta_{\kappa 0}\cos\delta_{\kappa 0}, f_{\kappa 1} = \cos\delta_{\kappa 0}, \kappa = 1, 2$.

When $0 < \delta_{\kappa 0} < \pi/2$, WMGB is in the stable operation range, and the derivative of $f_{\kappa 0}$ with respect to $\delta_{\kappa 0}$ can be obtained as follows:

$$
\frac{df_{\kappa 0}}{d\delta_{\kappa 0}} = \delta_{\kappa 0}\sin\delta_{\kappa 0} > \frac{df_{\kappa 0}}{d\delta_{\kappa 0}}(0) = 0, \quad \delta_{\kappa 0} \in \left(0, \frac{\pi}{2}\right) \tag{14}
$$

Thus, $f_{\kappa 0} > f_{\kappa 0}(0) = 0$. Further, it can be concluded that both $f_{\kappa 0}$ and $f_{\kappa 1}$ are greater than 0 when $0 < \delta_{\kappa 0} < \pi/2$.

Substitute Eq. (13) into Eq. (12), and it can be rewritten as:

$$
\begin{cases}
\ddot{\tilde{\delta}}_1 + \alpha_1\tilde{\delta}_1 - \beta_1\tilde{\delta}_2 + \gamma_1 = 0 \\
\ddot{\tilde{\delta}}_2 - \alpha_2\tilde{\delta} + \beta_2\tilde{\delta}_2 + \gamma_2 = 0
\end{cases} \tag{15}
$$

And the corresponding homogeneous equation of Eq. (15) is:

$$
\begin{cases}
\ddot{\bar{\delta}}_1 + \alpha_1\delta_1 - \beta_1\delta_2 = 0 \\
\ddot{\bar{\delta}}_2 - \alpha_2\delta + \beta_2\delta_2 = 0
\end{cases} \tag{16}
$$

with,

$$
\begin{aligned}
\alpha_1 &= f_{11}T_{M11}, \quad \beta_1 = f_{21}T_{M22}, \\
\gamma_1 &= f_{10}T_{M11} - f_{20}T_{M22} - T_{w\_eq} \\
\alpha_2 &= f_{11}T_{M12}, \quad \beta_2 = f_{21}T_{M21}, \\
\gamma_2 &= -f_{10}T_{M12} + f_{20}T_{M21} - T_{e\_eq}
\end{aligned}
$$

B. UNIFIED SOLUTION OF THE MOTION EQUATION BASED ON TAYLOR EXPANSION OF LOAD ANGLE

According to the theory of differential equations, the solution of Eq. (15) includes two parts: the general solution of homogeneous equation (16), and the special solution of Eq. (15), i.e.:

$$
\delta_\kappa = \bar{\delta}_\kappa + \delta_\kappa^* \tag{17}
$$

The general solution of the homogeneous equation (16) can be assumed as:

$$
\begin{cases}
\bar{\delta}_1 = a_1\sin(\omega_0 t + \varphi) \\
\bar{\delta}_2 = a_2\sin(\omega_0 t + \varphi)
\end{cases} \tag{18}
$$

where, a_1 and a_2 are the amplitudes; ω_0 and φ are the natural frequency and initial phase, respectively.

Substitute Eq. (18) into Eq. (16) to get:

$$
\begin{bmatrix}
\alpha_1 - \omega_0^2 & -\beta_1 \\
-\alpha_2 & \beta_2 - \omega_0^2
\end{bmatrix}
\begin{bmatrix}
a_1 \\ a_2
\end{bmatrix} =
\begin{bmatrix}
0 \\ 0
\end{bmatrix} \tag{19}
$$

When the system vibrates, system (16) has a nonzero solution, then the determinant of the coefficient matrix must be 0, i.e.:

$$
\omega_0^4 - (\alpha_1 + \beta_2)\omega_0^2 + (\alpha_1\beta_2 - \alpha_2\beta_1) = 0 \tag{20}
$$

It can be obtained from Eq. (20):

$$
\begin{cases}
\omega_{01}^2 = (C + D)/2 \\
\omega_{02}^2 = (C - D)/2
\end{cases} \tag{21}
$$

with $C = \alpha_1 + \beta_2 > 0, D = (\sqrt{(\alpha_1 - \beta_2)^2 + 4\alpha_2\beta_1}) > 0$. where, ω_{01} and ω_{02} are the 1st and 2nd natural frequency of system (16).

Combine Eqs. (12), (13), (16), and (21), we can get:

$$
C^2 - D^2 = (C + D)(C - D)
$$

$$= f_{11}f_{21}T_{M1}T_{M2} \cdot \frac{G_2N_{s1}N_{s2}J_h + p_{i2}N_{s1}J_m}{G_2J_lJ_mJ_h} > 0 \tag{22}$$

$C + D > 0$, so $C\text{-}D > 0$, $\omega_{01}^2 > \omega_{02}^2 > 0$, therefore, Eq. (20) has four roots: $\pm\omega_{01}$ and $\pm\omega_{02}$, we only take positive roots: ω_{01}, ω_{02}, and $\omega_{01} > \omega_{02}$.

Substitute ω_{01} and ω_{02} into Eq. (16), the 1st and 2nd main modes of the system are obtained as follows:

$$\begin{cases} \zeta_1 = \dfrac{a_1^{(1)}}{a_2^{(1)}} = \dfrac{\beta_1}{\alpha_1 - \omega_{01}^2} = \dfrac{\beta_2 - \omega_{01}^2}{\alpha_2} \\ \zeta_2 = \dfrac{a_1^{(2)}}{a_2^{(2)}} = \dfrac{\beta_1}{\alpha_1 - \omega_{02}^2} = \dfrac{\beta_2 - \omega_{02}^2}{\alpha_2} \end{cases} \tag{23}$$

Let $a_2^{(1)} = A_1$ and $a_2^{(2)} = A_2$, the general solution of homo-geneous differential equation (16) is calculated as follow:

$$\begin{cases} \bar{\delta}_1 = \zeta_1 A_1 \cos(\omega_{01}t + \Gamma_1) + \zeta_2 A_2 \cos(\omega_{02}t + \Gamma_2) \\ \bar{\delta}_2 = A_1 \cos(\omega_{01}t + \Gamma_1) + A_2 \cos(\omega_{02}t + \Gamma_2) \end{cases} \tag{24}$$

where, A_1, A_2, $\tilde{A}_1$, and $\tilde{A}_2$ are the undetermined coefficients, which can be determined by the initial conditions of the system (16).

Let $\delta_1^* = C_1$, $\delta_2^* = C_2$, and substitute them into Eq. (15), the special solution of Eq. (16) is calculated as follow:

$$\begin{cases} C_1 = -(\beta_1\gamma_2 + \beta_2\gamma_1)/(\alpha_1\beta_2 - \alpha_2\beta_1) \\ C_2 = -(\alpha_1\gamma_2 + \alpha_2\gamma_1)/(\alpha_1\beta_2 - \alpha_2\beta) \end{cases} \tag{25}$$

Based on the above analysis, the asymptotic solution of Eq. (12) can be obtained:

$$\begin{cases} \delta_1 = \zeta_1 A_1 \cos(\omega_{01}t + \Gamma_1) + \zeta_2 A_2 \cos(\omega_{02}t + \Gamma_2) + C_1 \\ \delta_2 = A_1 \cos(\omega_{01}t + \Gamma_1) + A_2 \cos(\omega_{02}t + \Gamma_2) + C_2 \end{cases} \tag{26}$$

Thus, the expression of magnetic torque of CMGs can be further obtained:

$$T_{mag\_\kappa} = T_{M\kappa} \sin\delta_\kappa \tag{27}$$

where, T_{mag_κ} is the magnetic torque of the κ^{th} CMG.

C. DYNAMIC PERFORMANCE CRITERIA -OVERSHOT

The stable operating points of system (15) can be easily obtained by analyzing its response expression Eq. (26):

$$\delta_{10}^* = -(\beta_1\gamma_2 + \beta_2\gamma_1)/(\alpha_1\beta_2 - \alpha_2\beta_1) \tag{28}$$

$$\delta_{20}^* = -(\alpha_1\gamma_2 + \alpha_2\gamma_1)/(\alpha_1\beta_2 - \alpha_2\beta) \tag{29}$$

It is noticed that$\delta_{10}^* = C_1$, $\delta_{20}^* = C_2$. In connection with Eq. (26), this also indicates that if WMGB is exerted by external nonlinear shock, its dynamic response is an oscillation near a pair of stable operating points.

To further determine the magnetic torque fluctuation of CMGs, it is necessary to evaluate the overshoot of the load angle and magnetic torque. The expression of overshoot of ϑ is given as follows:

$$Overshoot[\vartheta] = \max\{\vartheta_{\max} - \vartheta_0,\ \vartheta_0 - \vartheta_{\min}\}\big/\vartheta_0 \times 100\% \tag{30}$$

where, ϑ represents δ_κ or T_{mag_κ}; $\vartheta_{\max}$ and $\vartheta_{\min}$ are the max. and min. values of ϑ, respectively; ϑ_0 is the value at the stable operating point.

Then, the quantitative evaluation will be conducted based on Eq. (30) for the fluctuation of load angle and magnetic torque.

IV. MODEL VALIDATION AND DYNAMIC PERFORMANCE ANALYSIS

To validate the proposed analytical method based on load angle Taylor expansion, it is necessary to simulate the dynamic behavior of the proposed two-stage WMGB which parameters are listed in Table 1.

The operating condition of two-stage WMGB is complex and variable, especially the FSMG is extremely vulnerable to time-varying shock from the turbine rotor side. And due to the large-inertia and soft-magnetic characteristics of the transmission system, only the situation where the LS rotor angle changes suddenly are considered below [18]. Other situations will not be discussed specifically here.

Thus, two different states evaluation criteria are defined to represent the initial state of WMGB after being shocked by transient wind load:

$$State1 : \delta_1(0^+) = (1 + \chi)\delta_1(0^-) \tag{31}$$

$$State2 : \delta_1(0^+) = \delta_1(0^-) + \Delta\delta_1 \tag{32}$$

where, "0^-" and "0^+" are the very short time before and after the instantaneous shock, respectively. *State 1* indicates that the load angle δ_1 of FSMG becomes $(1+\chi)$ times after instantaneous shock. While *State 2* indicates that the load angle δ_1 of FSMG increases or decreases by $\Delta\delta_1$ after shock. The definitions of two different state evaluation criteria can be used to better evaluate the dynamic performance of the system and the change trend with various physical parameters.

To facilitate understanding, the flow chart of nonlinear dynamic analysis of WMGB based on load angle Taylor expansion is shown in Fig. 13. The specific analysis process includes four parts: *Modelling*, *Solution*, *Definition* and *Analysis*.

A. COMPARISON OF DYNAMIC RESPONSES OBTAINED BY R-K METHOD AND THE PROPOSED METHOD

To evaluate the effectiveness of the analytical method, the dynamic response of the two-stage WMGB is solved by R-K method and the proposed analytical method [28]. If the WMGB operates under rated operating conditions, when the transient shock (*State1*, and $\chi = 10\%$) occurs, the load angle and magnetic torque response of different CMGs can be obtained by the above two methods, as shown in

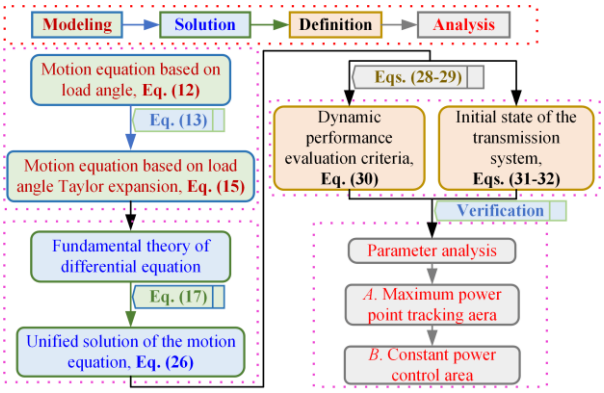

FIGURE 13. Flow chart of the proposed dynamic analysis method.

Fig. 14(a)-(d). For the convenience of observation, the magnetic torque in Fig. 14(c) and (d) are per unit values. From that, the solutions of load angle and magnetic torque based on R-K method is highly consistent with the proposed analysis method, but the proposed analysis method does not need to solve complicated differential equations and is more convenient to calculate. The load angle and magnetic torque have the same vibration frequency. And the dynamic responses of FSMG are sinusoidal, but the fluctuation of load angle and magnetic torque of SSMG are smaller than FSMG. According to Eq. (26), it can be obtained that the 1st mode ζ_1 is much greater than the 2nd mode ζ_2, thus, the influence of ζ_2 on FSMG can be ignored.

The influence of physical parameters on the dynamic performance of WMGB can be further analysed by Eq. (30). Thus, the variation law of the overshoot of load angle and magnetic torque under different operating conditions is studied.

B. DYNAMIC PERFORMANCE ANALYSIS AND EVALUATION

1) MAXIMUM POWER POINT TRACKING AREA ($V_{cut-in} \leq V < V_N$)

In this MPPT area, the wind speed V is less than rated wind speed V_N, so different wind speeds correspond to different driving torques T_w. Accordingly, the dynamic characteristics of the transmission system are also different when under different torque conditions. Therefore, it is necessary to evaluate the dynamic characteristics of the system under different torque conditions. The actual load capacity of WMGB related to T_w is defined as follows:

$$K_G = T_w / T_{N1} \tag{33}$$

where T_{N1} is the nominal torque of FSMG.

The change law of overshoot with different physical parameters is studied according to Eq. (30) based on R-K method and the proposed method. Thus, Fig. 15 and Fig. 16 show the change of overshoot with actual load capacity K_G under *State 1* ($\chi = 10\%$) and *State 2* ($\Delta\delta_1 = 2°$). From Fig. 15, K_G has little influence on the overshoot of load angle of CMGs under *State1*. This shows that when the external disturbance causes δ_1 to change with the same proportion, the correlation between the overshoot of the load angle and K_G can be ignored. Meanwhile, when K_G<0.4, the overshoot of magnetic torque changes slowly, while $K_G > 0.4$, the one decreases rapidly with the increase of K_G.

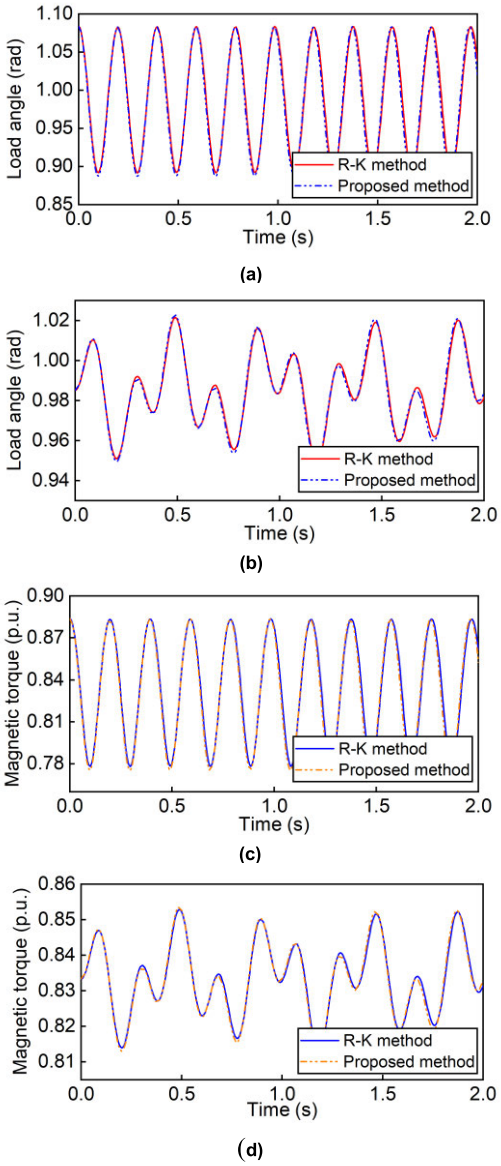

FIGURE 14. Comparison of load angle and magnetic torque under different solving methods. (a) load angle of FSMG, (b) load angle of SSMG, (c) magnetic torque of FSMG, and (d) magnetic torque of SSMG.

On the contrary, from Fig. 16, under *State 2*, when $K_G < 0.4$, the overshoot of both load angle and magnetic torque decreases rapidly with the increase of K_G, while $K_G > 0.4$, it changes very slowly. And the overshoot of load angle and magnetic torque of FSMG and SSMG are relatively close. Since the external disturbance directly exerts on the low-speed axis of the FSMG, the overshoot of its each parameter is always higher than that of the SSMG. From Fig.15 and Fig. 16, with the increase of K_G, the stable operating points of the system will be closer to the critical stable area

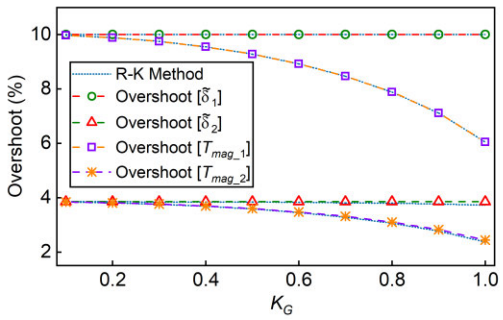

FIGURE 15. Relation between physical parameters and actual load capacity. (Under State 1).

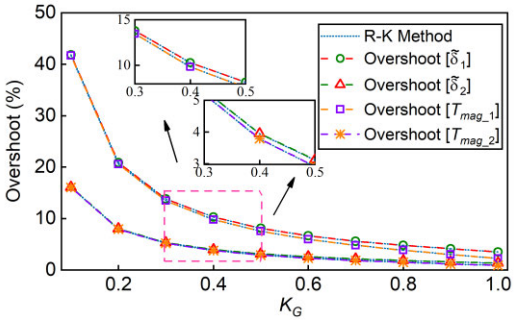

FIGURE 16. Relation between physical parameters and actual load capacity. (Under State 2).

in Fig. 8, and the operating performance of the system will also be more superior. It can be found that under normal light load conditions (especially $K_G > 0.5$), the overshoot of magnetic torque of all rotors are less than 10%; while under light-load conditions (especially near the cut-in wind speed), the overshoot of magnetic torque and load angle of FSMG is larger. In fact, the large overshoot only exists at the initial period of the work process. It can be concluded that the proposed two-stage WMGB can meet the requirements of wind power application.

2) CONSTANT POWER CONTROL AREA ($V_N \leq V < V_{cut-out}$)

In this area, the wind speed is less than the cut-out wind speed $V_{cut-out}$, the driving torques T_w will be controlled on purpose to keep at its rating. Thus, the design overload capacity of FSMG/SSMG has an important influence on the dynamic response of the system. The design overload capacity of the κ^{th} ($\kappa = 1, 2$) CMG is defined as follows:

$$K_\kappa = T_{M\kappa}/T_{N\kappa} \tag{34}$$

where, $T_{M\kappa}$ and $T_{N\kappa}$ are the stall torque and nominal torque of the κ^{th} CMG, respectively.

Here, K_κ is a system parameter, and its value will affect the inertia of different rotors directly. Assuming that there is a linear proportional relationship between inertia and design overload capacity K_κ, then the expression of the inertia of different rotors can be derived from Table 1:

$$\begin{cases} J_l = 95000K_1/3 \\ J_m = 200000K_1/7 + 100000K_2/21 \\ J_h = 12500K_2/3 \end{cases} \tag{35}$$

Similar to the analysis method in MPPT aera, Fig. 17 and Fig. 18 show the change of overshoot with design overload capacity K_1 and K_2 in the constant power control area. From Fig. 17, K_1 and K_2 have little effect on the overshoot of the load angle of the FSMG in *State 1*. As for the overshoot of magnetic torque of FSMG, its increase will slow down with the increase of K_1, but will not change with the variation of K_2. With the increase of K_1, the overshoot of the load angle and magnetic torque of SSMG decreases gradually, and then tends to a constant value. Contrarily, the overshoot of the

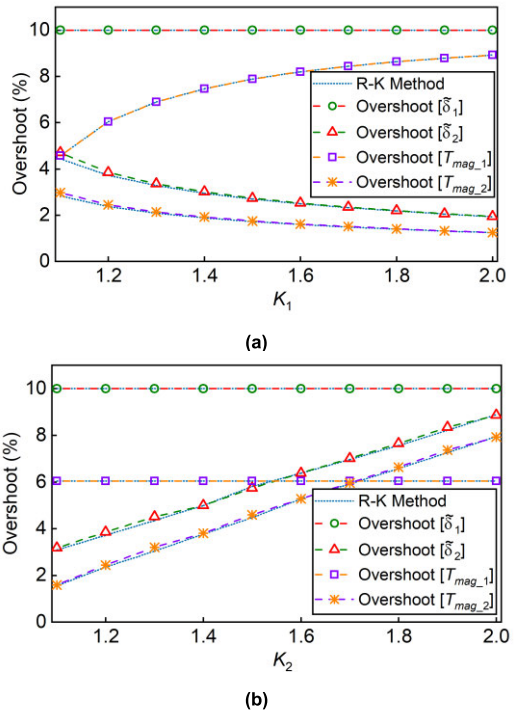

FIGURE 17. Relation between physical parameters and design overload capacity (Under State 1). (a) K_1, FSMG (b) K_2, SSMG.

load angle and magnetic torque of SSMG increases with the increase of K_2, which has a good linear relationship.

From Fig. 18, in *State 2*, the overshoot of load angle and magnetic torque of FSMG have a linear positive correlation with K_1, while those of SSMG do not change with K_1. Different from the abovementioned results, the overshoot of load angle and magnetic torque of SSMG have a linear positive correlation with K_2, while those of FSMG do not change with K_2. This also reflects that under *State 2*, the overshoot of the κ^{th} CMG is only affected by K_κ. Therefore, it can be concluded that both in *State 1* and *State 2*, the overshoot of FSMG is not affected by K_2.

C. DISCUSSION

According to the dynamic response results, the proposed model (15) can be conveniently to analyse the dynamic

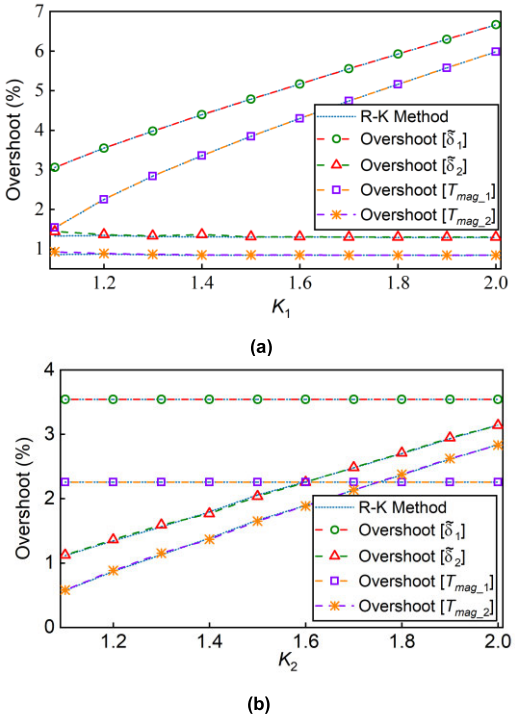

FIGURE 18. Relation between physical parameters and design overload capacity (Under State 2). (a) K_1, FSMG (b) K_2, SSMG.

TABLE 2. Comparison of two different analysis method.

Method	Operation speed	Accuracy	Solution type	Conclusion type	Scalability
R-K	Slow	Higher	Numerical	Qualitative	Weak
Proposed	Fast	High	Analytical	Quantitative	Strong

response of WMGB. Compared with (8), the dynamic responses can be applied directly by Eqs. (26) and (27) without solving complex differential equations, which improves the computational efficiency. Moreover, the natural frequency of the system can be easily obtained by the asymptotic expression (26), which provides raw data for the vibration analysis in the future.

The dynamic performance analysis results under different operating conditions shows that the results obtained by the proposed method are consistent with those obtained by R-K method. From Fig. 15 to Fig. 18, in the normal operating area, the overshoot of magnetic torque is less than 10%, which also verifies the effectiveness of two-stage WMGB applied to wind turbines [29]. In addition, the conclusions obtained from the dynamic performance analysis can provide a basis for the re-optimization of WMGB.

In addition, the definition of performance and state evaluation criteria makes it convenient to quantitatively analyse the dynamic performance of WMGB. In this paper, only the case of the changing of load angle is studied when subjected to transient shock. However, according to the general steps of the proposed analysis method, the study scope can be extended to other cases, such as the dynamic performance analysis under sinusoidal load disturbance.

Finally, a comparison between the proposed method and the R-K method is shown in Table 2.

V. CONCLUSION

This article presents a nonlinear analytical approach for evaluating the dynamic characteristic of the multistage magnetic gearbox for wind turbine. And the following conclusions can be drawn:

1. The dynamic performance of magnetic gearbox varies due to the changes of operating conditions. Especially under constant load angle disturbance, the overshoot of magnetic torque of every coaxial magnetic gear is only affected by its own design overload capacity and has a good linear relationship. In addition, the analysis result also verifies the feasibility of magnetic gearbox applied to wind turbines and provide a basis for its re-optimization.
2. It is necessary and effective to define the performance and state evaluation criteria for quantitative evaluation of the dynamic performance of magnetic gearbox. This paper only considers the case where the load angle of first-stage coaxial magnetic gear changes when subjected to transient shock. However, according to the proposed method, the analysis scope can be extended to other cases.
3. Reviewing the solution process, the proposed method in this paper can directly obtain the dynamic response of load angle and magnetic torque by the asymptotic expressions, which simplifies the analysis process. In addition, the dynamic response result verifies the accuracy of the proposed method and the rationality of the two-stage WMGB applying to the wind power generation system. Due to the sophisticated dynamic characteristics of the multistage magnetic gearbox, its system-level control feed into the actual operating conditions is considered a challenge. Thus, a dynamic performance study considering the influence of controller will be conducted in future work.

REFERENCES

[1] X. Chu, "Multiobjective design and performance analysis of the ultra-low speed axial flux disc motor for maglev wind yaw system," *IEEE Trans. Ind. Electron.*, vol. 69, no. 4, pp. 3471–3480, Apr. 2022.

[2] Y. Aafif, A. Chelbi, L. Mifdal, S. Dellagi, and I. Majdouline, "Optimal preventive maintenance strategies for a wind turbine gearbox," *Energy Rep.*, vol. 8, pp. 803–814, Nov. 2022.

[3] E. Gouda, S. Mezani, L. Baghli, and A. Rezzoug, "Comparative study between mechanical and magnetic planetary gears," *IEEE Trans. Magn.*, vol. 47, no. 2, pp. 439–450, Feb. 2011.

[4] R.-J. Wang and S. Gerber, "Magnetically geared wind generator technologies: Opportunities and challenges," *Appl. Energy*, vol. 136, pp. 817–826, Dec. 2014.

[5] Y. Wang, M. Filippini, N. Bianchi, and P. Alotto, "A review on magnetic gears: Topologies, computational models, and design aspects," *IEEE Trans. Ind. Appl.*, vol. 55, no. 5, pp. 4557–4566, Sep. 2019.

[6] K. Tsurumoto and S. Kikuchi, "A new magnetic gear using permanent magnet," *IEEE Trans. Magn.*, vol. MAG-23, no. 5, pp. 3622–3624, Sep. 1987.

[7] K. Atallah and D. Howe, "A novel high-performance magnetic gear," *IEEE Trans. Magn.*, vol. 37, no. 4, pp. 2844–2846, Jul. 2001.

[8] M. C. Gardner and H. A. Toliyat, "Nonlinear analysis of magnetic gear dynamics using superposition and conservation of energy," in *Proc. IEEE Int. Electr. Mach. Drives Conf. (IEMDC)*, May 2019, pp. 210–217.
[9] A. B. Kjaer, S. Korsgaard, S. S. Nielsen, L. Demsa, and P. O. Rasmussen, "Design, fabrication, test, and benchmark of a magnetically geared permanent magnet generator for wind power generation," *IEEE Trans. Energy Convers.*, vol. 35, no. 1, pp. 24–32, Mar. 2020.
[10] K. Li, S. Modaresahmadi, W. B. Williams, J. D. Wright, D. Som, and J. Z. Bird, "Designing and experimentally testing a magnetic gearbox for a wind turbine demonstrator," *IEEE Trans. Ind. Appl.*, vol. 55, no. 4, pp. 3522–3533, Jul. 2019.
[11] K. Atallah, J. Rens, S. Mezani, and D. Howe, "A novel 'Pseudo' direct-drive brushless permanent magnet machine," *IEEE Trans. Magn.*, vol. 44, no. 11, pp. 4349–4352, Nov. 2008.
[12] L. Jian, K. T. Chau, and J. Z. Jiang, "A magnetic-geared outer-rotor permanent-magnet brushless machine for wind power generation," *IEEE Trans. Ind. Appl.*, vol. 45, no. 3, pp. 954–962, Jun. 2009.
[13] W. N. Fu and S. L. Ho, "A quantitative comparative analysis of a novel flux-modulated permanent-magnet motor for low-speed drive," *IEEE Trans. Magn.*, vol. 46, no. 1, pp. 127–134, Jan. 2010.
[14] Q. Qin, Y. Qiu, and B. Cai, "Optimization design and dynamic characteristics analysis of multistage magnetic gearbox for MW-scale wind turbine," *J. Electr. Eng. Technol.*, vol. 18, no. 4, pp. 2969–2981, Jul. 2023.
[15] X. Zhang, J. Zhong, W. Li, and M. Bocian, "Nonlinear dynamic analysis of high-speed gear pair with wear fault and tooth contact temperature for a wind turbine gearbox," *Mechanism Mach. Theory*, vol. 173, Jul. 2022, Art. no. 104840.
[16] S. Li and W. Xu, "Vibration analysis of permanent magnet synchronous motor using coupled finite element analysis and optimized meshless method," *Nonlinear Dyn.*, vol. 108, no. 1, pp. 167–189, Mar. 2022.
[17] R. G Montague, C. M Bingham, and K. Atallah, "Magnetic gear dynamics for servo control," in *Proc. Melecon 15th IEEE Medit. Electrotech. Conf.*, Apr. 2010, pp. 1192–1197.
[18] C.-L. Chen and M.-C. Tsai, "Kinematic and dynamic analysis of magnetic gear with dual-mechanical port using block diagrams," *IEEE Trans. Magn.*, vol. 54, no. 11, pp. 1–5, Nov. 2018.
[19] P. Tzouganakis, V. Gakos, C. Kalligeros, A. Tsolakis, and V. Spitas, "Fast and efficient simulation of the dynamical response of coaxial magnetic gears through direct analytical torque modelling," *Simul. Model. Pract. Theory*, vol. 123, Feb. 2023, Art. no. 102699.
[20] X. Liu, Y. Zhao, X. Zhang, J. Gao, and S. Huang, "Investigation of the dynamic characteristics of a coaxial magnetic gear under loading condition based on analytical model," in *Proc. 20th Int. Conf. Electr. Mach. Syst. (ICEMS)*, Aug. 2017, pp. 1–5.
[21] I. Marinova and V. Mateev, "Modeling of dynamic torque control of a coaxial magnetic gear," in *Proc. 22nd Int. Conf. Comput. Electromagn. Fields (COMPUMAG)*, Jul. 2019, pp. 1–4.
[22] B.-E.-B. Bidouche, T. Lubin, and S. Mezani, "Dynamic behaviour of a magnetically geared induction machine," in *Proc. 19th Int. Symp. Electromagn. Fields Mechatronics, Electr. Electron. Eng. (ISEF)*, Aug. 2019, pp. 1–2.
[23] S. Hartung and I. Rehberg, "Dynamics of a magnetic gear with two cogging-free operation modes," *Arch. Appl. Mech.*, vol. 91, no. 4, pp. 1423–1435, Apr. 2021.
[24] L. Xu and X. Zhu, "Natural frequencies and vibrating modes for a magnetic planetary gear drive," *Shock Vibrat.*, vol. 19, no. 6, pp. 1385–1401, 2012.
[25] S. J. Kim, E.-J. Park, S.-Y. Jung, and Y.-J. Kim, "Transfer torque performance comparison in coaxial magnetic gears with different flux-modulator shapes," *IEEE Trans. Magn.*, vol. 53, no. 6, pp. 1–4, Jun. 2017.
[26] M. Desvaux, R. L. G. Latimier, B. Multon, S. Sire, and H. Ben Ahmed, "Analysis of the dynamic behaviour of magnetic gear with nonlinear modelling for large wind turbines," in *Proc. 22nd Int. Conf. Electr. Mach. (ICEM)*, Sep. 2016, pp. 1332–1338.
[27] S. Gerber and R.-J. Wang, "Cogging torque definitions for magnetic gears and magnetically geared electrical machines," *IEEE Trans. Magn.*, vol. 54, no. 4, pp. 1–9, Apr. 2018.
[28] R. Ding, H. Zhang, D. Xu, C. Liu, Q. Shi, J. Liu, W. Zou, and Y. Wu, "Experimental and numerical study on motion instability of modular floating structures," *Nonlinear Dyn.*, vol. 111, no. 7, pp. 6239–6259, Apr. 2023.
[29] L. Xu, C. Zhu, H. Liu, G. Chen, and W. Long, "Dynamic characteristics and experimental study on a wind turbine gearbox," *J. Mech. Sci. Technol.*, vol. 33, no. 1, pp. 393–402, Jan. 2019.

QINGHAI QIN received the B.S. degree in packaging engineering from Qufu Normal University, Rizhao, China, in June 2020, where he is currently pursuing the M.S. degree in control science and engineering with the College of Engineering.

His current research interests include the optimization design and dynamic analysis of magnetic gears.

BIN CAI received the Ph.D. degree in electrical engineering from Xi'an Jiaotong University, Xi'an, China, in 2004.

He is currently a Professor with the College of Engineering, Qufu Normal University, Rizhao, China. His current research interests include wind power generation and the applications of artificial intelligence in the renewable energy control fields, power electronics, and HVDC-flexible transmission technology.

YUCHENG DU received the B.S. degree in electrical engineering and its automation from Qufu Normal University, Rizhao, China, in June 2021, where he is currently pursuing the M.S. degree in electrical engineering with the College of Engineering.

His current research interest includes the power control of vertical-axis wind turbines.